Performance Evaluation Of DFTB1 And DFTB2 Methods In Reference To The Crystal Structures And Molecular Energetics Of Siloxaalkane Molecular Compass

Anant Babu Marahatta[1*]

[1]Professor of Chemistry, Engineering Chemistry and Applied Science Research Unit, Departments of Civil, Computer and Electronics Engineering, Kathford Int'l College of Engineering and Management (Affiliated to Tribhuvan University), Kathford Int'l Education & Research Foundation, Lalitpur, Nepal

*Corresponding author: abmarahatta@gmail.com/anant.marahatta@kathford.edu.np

Abstract – In the lately developed computational paradigms and state-of-art theoretical analyses, the density-functional based tight-binding (DFTB) scheme and its profound theoretical features extended to address the crystalline molecular systems stand as the most versatile quantum mechanical method. Being its computational parser codes extremely efficient and even assessable directly as a low-cost scheme despite hosting *ab initio* functionalities comprising mathematical formulations, the "non-self-consistent-charge" (DFTB1) and "self-consistent-charge" (DFTB2) approaches are extensively applied to the wide ranged molecular systems under both crystalline (PBC) and non-crystalline conditions. The "dispersion energy corrections (DECs)" features of it further add an additional value to their rational applications. Herewith, the intensive evaluations on their performances are carried out based on the results they produced for the experimentally synthesized amphidynamic type molecular crystal with macroscopic compass like supramolecular assembly possessing central dipolar difluorophenylene rotator (compass needle), axial Si−C bond spin axis, and peripheral −Si− & −Si−O− made siloxaalkane stator. It is found that the DFTB2 performed far better than the DFTB1 in reference to its datasets: (a) lengths for the bonds associated with rotator, stator, and spin axis, (b) free−volume unit around the rotator, (c) rotational energy barriers, viz. E_a= 5.99 kcal/mol, & 5.52 kcal/mol under PBC with and without DECs, and (d) locations of the 1π−flipped (rotator) degenerate equilibrium structures, viz. at ϕ = 0.505π & 1.493π (*Expt.* ϕ = 0.56π & 1.56π) radians. Besides this, the dispersion constants for the F atom; cutoff r_c=3.8Å, polarizability α =3.4Å^3, and effective nuclear charge Z^*=3.5au determined by DFTB2, and the precise unit-cell geometries derived by undertaking these numeral values further exemplified its superiority over DFTB1. It is believed that all the justifications and quantitative interpretations conferred throughout this article put considerable demands on the accuracy of DFTB2 for investigating crystal structures and molecular energetics explicitly.

Keywords – DFTB$^+$, Dispersion energy constants, Potential energy surface, Activation energy barrier E_a

I. INTRODUCTION

Over the last decade, the experimentally synthesized and computationally designed prototype molecular model with a bridged dipolar or non-polar π−electronic system as a mobile unit linked externally to the static yet flexible type peripheral spokes via the spin axis (Fig.1(A)) have gained substantial attentions in the nanometric world [1,2]. As a fundamental element of nanotechnology and molecular machine, such macrocyclic supramolecular type molecular model possessing a completely closed three dimensional structural topology and an ideally unique amphidynamic behavior has actually triggered the scientists around the world not only due to exhibiting various propitious yet functionalizable physicochemical properties [1−4] but also to its typical working mechanisms and operational principles resembling closely to that of the macroscopic compass and gyroscope, respectively called crystalline molecular compass and gyroscope [3−6]. Among these promising molecular modules for the future

nano−machines, the crystalline molecular compass architected with the potent static arms encompassing a dipolar phenylene ring attached to the electronegative atoms/groups (compass needle) at ortho and meta positions vows more to the fundamental norms of nanotechnology and nanoscale machinery such as (a) exhibiting external− stimuli controlled rotary motion by conserving internal volume, (b) demonstrating dichroism and birefringence type fascinating optical phenomena, (c) designing functional crystalline free molecular machine at room temperature, (d) creating smart yet responsive nanomaterials, etc. [7−11]. In the year 2007, the esteemed research group led by W. Setaka accomplished the complete strategical synthesis of similar type macrocyclic crystalline molecular compass (orthorhombic, number of molecules per unit−cell $Z = 4$) with −Si− and $(-Si-O-)_x$ made flexible yet robust siloxa- alkane spoke (each arm is represented by an arch in Fig.1(A)) encapsulating the dipolar ortho-meta-
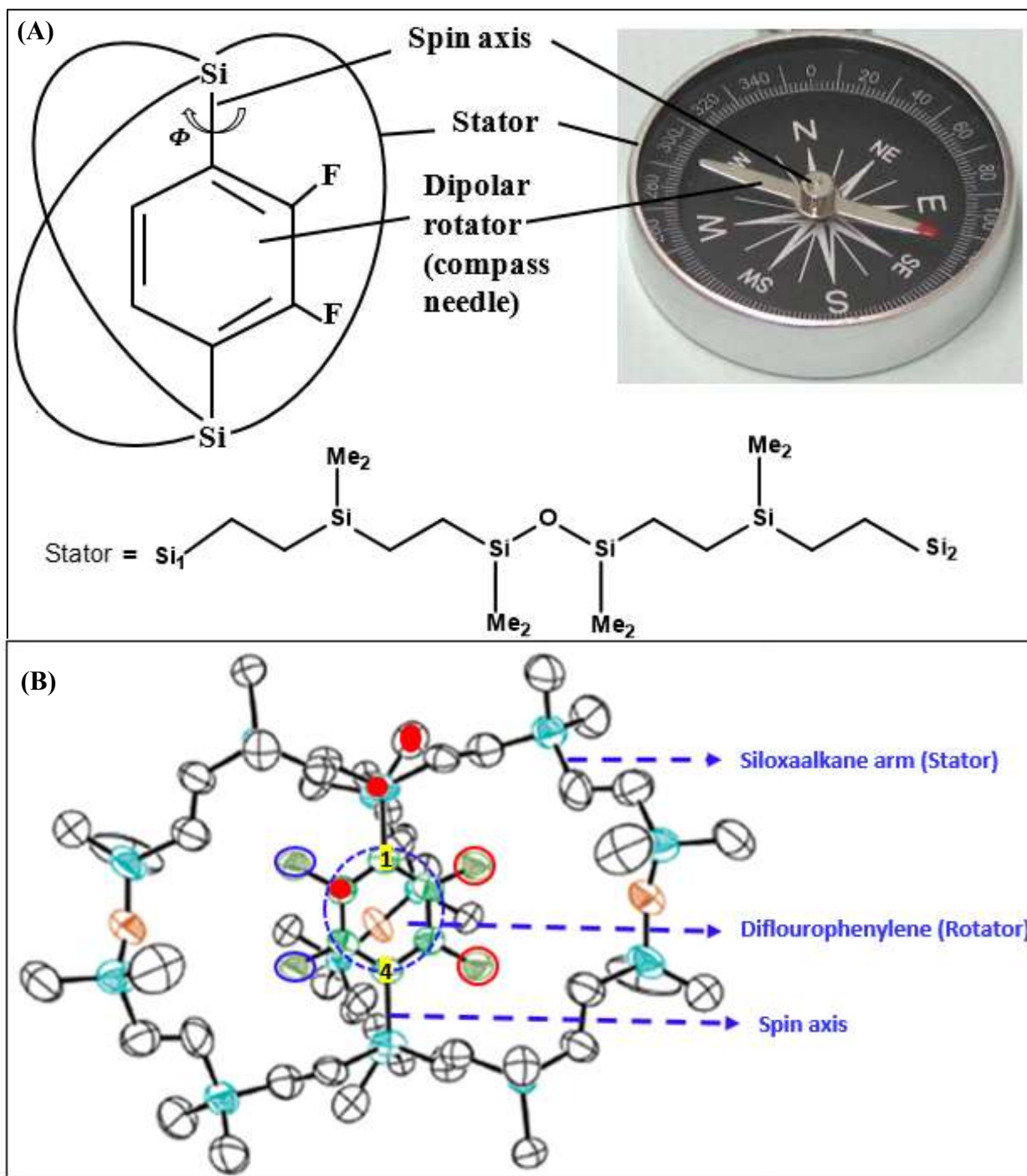
Fig.1. (A) A mobile dipolar π-electronic system bridged prototype molecular model with three static yet flexible peripheral arms (represented by three arcs; the chemical constituents of each arc used to synthesize ROT−2F molecule B are also shown), (B) An X−ray crystallography of siloxaalkane molecular compass ROT−2F with three explicit siloxaalkane arms encompassing difluorophenylene dipolar rotator (compass needle) linked to the C1 and C4 based spin axis (C−Si bond). The experimentally observed two stable degenerate 1π−flipped positions of the rotator inside the static spokes are marked by blue and red colored line-spheroids. The dihedral angle ϕ used for evaluating unit-cell geometries and calculating potential energy surfaces (PESs) is defined by the C atom of the siloxaalkane arm (red color filled spheroid), Si atom of the spin axis (red color filled spheroid), *ipso* C1 (shaded by yellow color) and *ortho* C (red color filled spheroid) atoms of the rotator.

difluorophenylene segment (a compass needle) (hereafter, ROT−2F) centrally by creating sufficient free−volume unit (it approximates the free space available around the rotating segment) [12,13]. By the X−ray crystallography and ^{1}H NMR spectroscopy, they observed (a) smooth 1π−flipped positions of the difluorophenylene ring along its C1 and C4 linked Si−C bond spin axis, (b) degenerate 1π−flipped molecular structures with 0.5:0.5 occupancy factor, and (c) a completely static yet flexible type siloxaalkane spokes; at temperature as equal as 298 K in solution phase [13]. Just for the reference, the X−ray derived molecular structure of ROT−2F with 1π− flipped difluorophenylene (rotator) positions is shown in Fig. 1(B) where all the designated compass parts are labeled. In the year 2010 and onwards, the research works led by H. Kono and the present author himself verified all those experimentally reported optimistic yet realistic structural and dynamical observations theoretically and computationally [14−18]. Therewith, the structural deformations and degeneracies, siloxaalkane arms elongations, strategical molecular architectures, thermodynamic viewpoints of the site occupancy, real time rotary dynamics, etc. were critically analyzed, and presented the experimentally unrevealed rotary parameters such as free−volume unit, flipping barriers E_a, nature of the rotational potential energy surfaces, flipping rates at wide ranged kinetic temperatures, etc. quantitatively. The genuine quantum mechanical methods and the esteemed computational methodologies that the authors employed therewith were "non-self-consistent-charge" NCC (hereafter, DFTB1) [19] and "self-consistent-charge" SCC (hereafter, DFTB2) [20] approaches of the extended density-functional-based tight-binding (herewith, DFTB$^+$) method [21−23] plus their externally driving and *Gaussian* interface routing *Gaussian−external* methodology [14, 15, 24]. Despite granting many remarkable dissimilar results and generating quantum mechanically distinctive geometrical and dynamical descriptors while applying each of them explicitly to the ROT−2F molecular compass under isolated and crystalline (periodic boundary condition (hereafter, PBC)) conditions with and without "dispersion energy corrections", the present author selectively reported therewith the results derived by the DFTB2 methods only. Nowhere the limitations of DFTB1 over DFTB2 are underscored along with the in− depth criticisms on their individual performances, computing abilities, and distinctive mathematical formulations. In this regard, present research report puts significant value. Towards finding out the leading DFTB method targeted to address the crystalline molecular assembly wholly, this report is believed to act as a stepping−stone. Additionally, the significance of implementing "dispersion energy corrections" features (van der Waals interactions (both intra− and inter− molecular) under DFTB2, and the improvements on its computing abilities while doing so can also be assessed here thoroughly. In the support of the same, the quantitatively validated and practically examined dispersion constants such as polarizability α (Å^3), cutoff r_c(Å), Slater− Kirkwood effective numbers N_{eff} of electrons, and effective nuclear charges Z^* for the specific atom/s [25−27], and their secret roles in determining relatively more accurate molecular geometries and ground state energies of such a complex crystalline ROT−2F molecular assembly are also presented.

As the DFTB1 and DFTB2 schemes have uniquely yet distinctly modeled mathematical formulations: (a) the former is a standard zeroth−order and the latter is a standard second−order expansions of the Kohn−Sham total energy in DFT with respect to charge density fluctuations [22, 23]; (b) the former is a traditional type NCC tight-binding (TB) approach in which no explicit interatomic charge interactions terms are included, and the concerned eigenvalue of the Hamiltonian operator is a result of the noniterative computations, it is applicable mainly to the nonpolar and homonuclear systems such as carbon fullerene isomers [28a], transition metal catalyzed carbon nanotube formation procedures [28b], etc.; and the latter is an iterative SCC method that treats the charge distribution in a molecule (point charges) by taking into account the interatomic charge interactions, it is relatively more useful to the wide range molecular systems but is usually recommended to the heteroatomic one where the charge balance between the atoms is crucial [20]; (c) the latter method always derives relatively more transparent, parameter−free, and readily solvable mathematical expressions for the generalized Hamiltonian matrix constructed through the nearest neighbor relationships, often incorporates the Mulliken charges into its SCC procedure fully, and computes the corresponding nuclear forces with significant accuracy, the proper inclusions of the "dispersion energy corrections" algorithms in it under PBC sounds more meaningful than that carrying out through the former, their explicit employments in different type molecular systems obviously produce significantly varied results. Reiteratively saying, the latter approach is specifically designed for the precise implementation of Slater−Kirkwood dispersion model [25] responsible to account for the predominant dispersion energies (intermolecular and intramolecular type van der Waals interactions) exist in the macrocyclic supramolecular crystalline systems, and for the exact execution of Slater−Koster files (SK−files) with a focus on solid state systems [29] plus for the accurate improvisations of in-built deficiencies of the former, their unanimous abilities to treat the complex molecular systems quantum mechanically are apparently distinguishable even though they produce the results their level standards (competitive to that of the

DFT (6–31$G(d)$) [28], and other high-level *ab initio* & first principle methods [30] plus semiempirical AM1 and PM3 [31]) but non–reproducible to each other. Therefore, it is meaningful to evaluate their individual performances and computing abilities while applying separately to the same crystalline molecular assembly (in this case, ROT–2F type heteroatomic amphidynamic crystalline molecular systems), and to present their rigorous yet deterministic perspectives quantitatively. Herewith, in the course of evaluating them quantitatively, present author has reproduced nominal structural datasets from his original publications [15, 16]. This research paper is structured as: in section 2; computational methods, in section 3; results and discussions, in section 4; summary and conclusions.

II. COMPUTATIONAL METHODS

Out of the two X–ray diffraction observed 1π–flipped degenerate equilibrium structures of ROT–2F (occupancy factors = 0.5:0.5) whose dihedral angles ϕ (angle between the diflourophenylene rotator and a reference plane of the siloxaalkane arm) (the complete definition of ϕ is given in Fig. 1(B)) were measured as 0.56π, and 1.56π respectively, the Cartesian atomic coordinates of the former position were taken here as a trial structure (unit–cell). The required crystallographic information such as crystal lattice, unit–cell parameters (edges of the unit–cell (lattice vectors) a, b, and c, and the angles between them α, β, and γ), etc. were extracted from the Mercury crystallographic software [32(a)] accessible *.cif* extended files, and the concerned dihedral angles were measured in the *Jmol* [32(b)] rendered X–ray derived unit–cell. The trial structure with $\phi = 0.56\pi$ was optimized by both DFTB2 and DFTB1 methods under PBC (PBC = Yes) with and without "dispersion energy corrections", and analyzed their equilibrium structures quantitatively with the explicit geometrical comparisons. Prior to optimizing this trial structure under PBC, the isolated molecule of ROT–2F was optimized by DFTB1 and DFTB2 separately under non–crystalline condition (PBC = No), and examined their structural convergence abilities in reference to the geometrical parameters and the structural alignments of its static siloxaalkane arms, central rotating diflourophenylene segment, and the orientation of other substituents plus steric hindrance creating bulky groups in the three dimensional space. The specific DFTB$^+$ keywords responsible for driving these computational schemes under PBC = Yes/No options such as Hamiltonian matrix elements, lattice optimization technique, Brillouin zone integration process, molecular symmetry breakage blocking strategy, Cartesian coordinates incorporating drivers, SCC/NCC iterations enforcing mathematical formulations, van der Waals forces' addressing Slater–Kirkwood polarization atomic model, dispersion constants incorporating computational routes, Slater–Koster (SK) files accessing quantum mechanical pathways, etc., and the detailed technical aspects of their operational procedures were assessed from the original publications of the same author [14,15]. The additional DFTB1 and DFTB2 parametrizations, and the crystalline solid state targeted extended features accessing computational parser codes were adopted from the DFTB$^+$ manual [33].

Besides undertaking the geometrical parameters for evaluating computing abilities of the DFTB1 and DFTB2 methods, their quantum mechanically produced molecular energies (potential energy surface PES) under PBC = Yes with and without "dispersion energy corrections" at each specific dihedral angleϕ of the rotator constrained programmatically via the *Gaussian* keyword "*ModRedundant*" were also taken into account. The dispersion constants values for the H, C, Si, and O atoms of ROT–2F molecule such as polarizability α (Å^3), cutoff r_c (Å), Slater–Kirkwood effective numbers N_{eff} of electrons, and effective nuclear charges Z^* required to incorporate the effects of van der Waals dispersion energy were set based on the clarifications and recommendations given elsewhere [14, 33, 34], and those constants for the F atom were determined here quantum mechanically. While scanning the PES by each of these methods, the rotational angle of the difluorophenylene rotator was scaled up clockwise and anticlockwise from the original $\phi = 0.56\pi$ radian, and computed the specific Eigen value at each constrained dihedral angle by letting other degrees of freedom fully relaxed. Since this type of the computational technique cannot be carried out routinely via either of these two DFTB alone schemes, the *Gaussian's* PES scanning procedures with Berny geometry *optimization* algorithm [35] were put into effect via the "*Gaussian–External*" methodology [14, 15]; a programmatic scheme that calls these scanning features computationally via the users provided "External script", and runs the desired DFTB codes in *Gaussian* interface via the keyword "*External*".

III. RESULTS AND DISCUSSIONS

3.1 Performance Evaluations of DFTB1 and DFTB2 Methods

3.1.1 In reference to Optimized Geometries under Non−crystalline (Isolated) Condition

In the theoretical and computational studies, the *ab initio* and DFT methods based deterministic approaches always provide benchmark structural interpretations over all the semi− empirical based quantum mechanical approximations. Therefore, herewith, the X−ray derived molecular geometry of the ROT−2F was at first optimized by DFT: B3LYP/6−31G (*d, p*) method under isolated condition (PBC=No), and compared most of their structural descriptors with those of the DFTB1 and DFTB2 predicted datasets. The descriptors that were chosen here selectively include all the accessory compass parts of the ROT−2F molecular compass: rotator, stator, and spin axis, and its few more gyroscopic/compass credentials: "free−volume" unit, and "dihedral angle" that depicts free space around the rotator and its angle of orientation in respect to peripheral siloxaalknae arm respectively. In the periphery of the same, the geometry convergence abilities and low energy ground state equilibrium structures searching skills of the DFTB1 and DFTB2 are examined. The concerned datasets (bond lengths (nm) and bond angles (π rad.)) for each of these compass parts and the geometrical descriptors are summarized in Table 1; where the DFT, DFTB1, DFTB2 predicted values are mentioned explicitly. As can be seen there itself, all these quantum mechanical methods predicted the bond lengths (*l*) for C−F, C−C, and C−H associated with the central difluorophenylene rotator in the range of 0.14nm, 0.14nm, and 0.11nm respectively. They are almost in the agreeable range with those of the X−ray derived distances. While referring to the C−C ($l_{c-c} = 0.147$nm), and C=C bond lengths ($l_{C=C} = 0.135$nm) of the non-substituted standard phenylene ring, all those methods predicted C−C bond length value of the difluorophenylene rotator are found to be in the intermediate range, describing its partial double bond characters and the delocalized behavior of electrons (degree of aromaticity). Towards this aromaticity revealing plus the degree of closeness with that of the X−ray and DFT derived datasets, the DFTB2 derived values seem more precise. Similarly, while referring to the theoretically computed bond lengths C−C, C−H,

Table 1. Comparison between DFTB1 and DFTB2 optimized structural parameters of the ROT−2F molecular compass under isolated molecular condition (non-crystalline condition).

| Molecular Compass (ROT−2F)	Bond lengths (nm)	Experimental/Theoretical methods (PBC = No)			
		X−ray	DFT	DFTB1	DFTB2
Rotator (difluorophenylene)	C−F	0.144	0.141	0.138	0.141
	C−C	0.138	0.139	0.140	0.136
	C−H	0.093	0.110	0.110	0.110
Stator (Siloxaalkane arm)	C−C	0.153	0.153	0.154	0.152
	C−H	0.097	0.110	0.109	0.109
	C−Si	0.188	0.187	0.188	0.191
	Si−O	0.163	0.175	0.176	0.172
	∠Si−O−Si (avg.)	0.88π	0.76π	0.76π	0.77π
Spin axis	C1−Si1	0.189	0.187	0.188	0.189
	C4−Si2	0.189	0.187	0.188	0.189
"Free−volume" (d_{OF}) (*nm*)	*d1*	0.510	0.480	0.507	0.481
	d2	0.840	0.851	0.854	0.848
	d3	0.950	0.920	0.918	0.923
Rotator's dihedral angle (ϕ)	All the atoms involved to form this dihedral angle are defined in Fig. 1	0.56π	0.63π	0.68π	0.63π
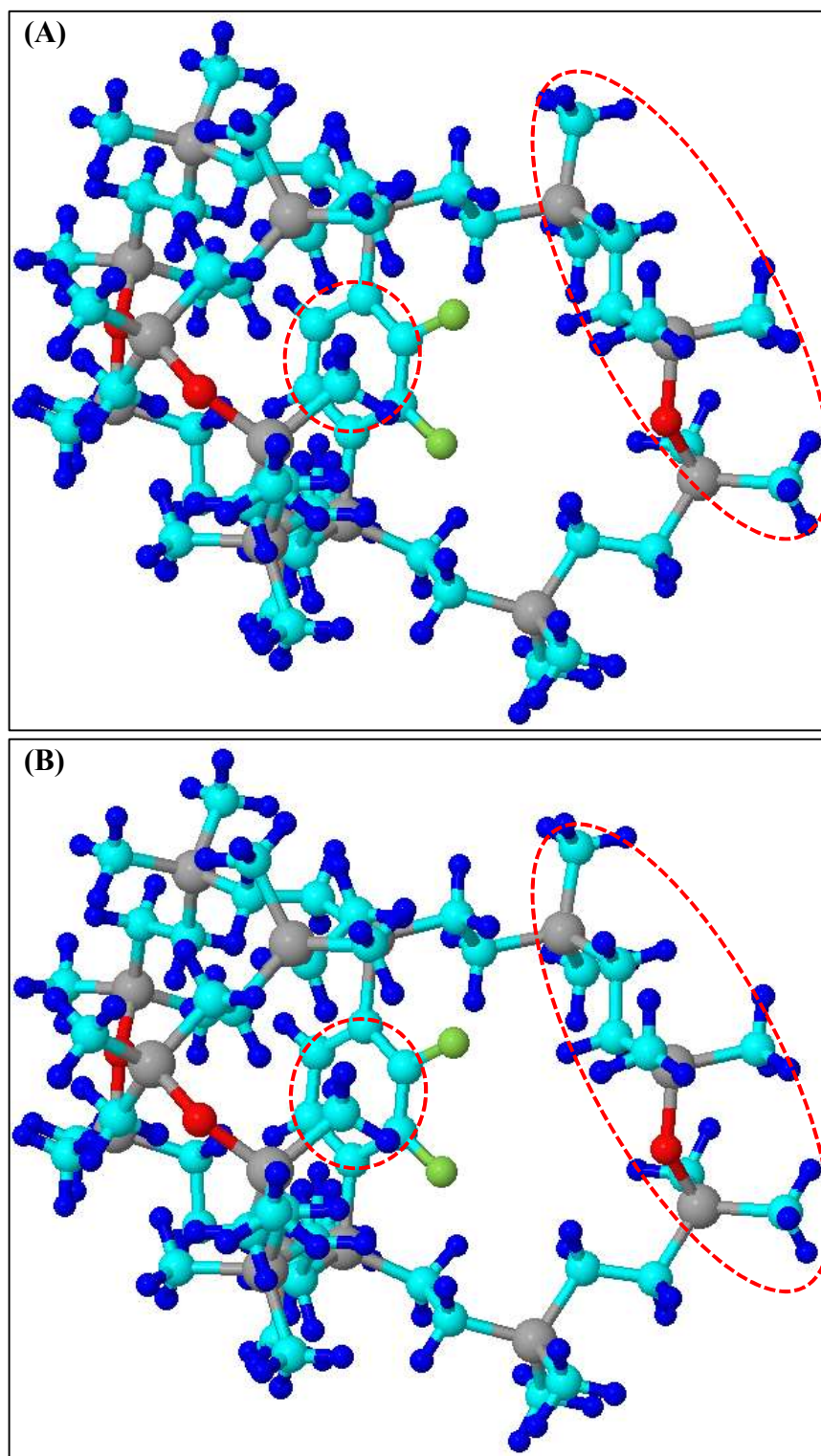
Fig.2. The *Jmol* rendered (**A**) DFTB1, and (**B**) DFTB2 optimized electronic structures of ROT−2F molecular compass under non-crystalline (isolated molecular) condition. The green, blue, dark gray, red, and cyan spheroids represent F, H, Si, O, and C atoms respectively. The compass parts such as central dipolar difluorophenylene rotator and a peripheral siloxaalkane stator are encircled by the red colored shapes.

C−Si, and Si−O plus Si−O−Si bond angles associated with each siloxaalkane arm (stator), they are respectively found in the range of 0.15 nm, 0.10 nm, 0.19 nm, 0.17 nm, and 0.76π radian. All these distances except estimated to the $(-Si-O-)_x$ segments are closely resembled to those of the X−ray produced datasets. The significant discrepancies observed mainly in the Si−O bonds and Si−O−Si bond angles are because of the partial ionic and double bond characters of the −Si−O−Si− linkages which is however, responsible in providing extra strength to the siloxaalkane arms, and in contributing exceptional conformational flexibility [36]. But, it is quite obvious while considering the in−built quantum mechanical formulations of even the DFT and DFTB2 methods as they are still suffering from the complete mathematical incorporations of the effects of partial π−double bond characters plus the van der Waals type intramolecular interactions (interactions between the central rotator and peripheral stator) in their those type computational procedures that are carried out under non−crystalline and non−dispersion energy correction conditions (isolated molecular condition) [37]. Again, on the basis of theoretically determined lengths of the C_1-Si_1 (0.19nm) and C_4-Si_2 (0.19nm) (Fig. 1(b)) bond spin axis along which the rotator exhibits facile 1π flipping motion centrally, all the three theoretical methods are found to perform very satisfactorily. But, more precise is the DFTB2 as it produces the X−ray derived spin axis bond length more consistent than that by the DFTB1. Moreover, in terms of free−volume unit $d_{OF} = \{d1, d2, d3\}$ (the intervening space exists in between O atom of each siloxaalkane arm (there are in total three siloxaalkane arms in each molecule) and the nearest F atom of the central difluorophenylene rotator) estimated in all the three theoretically optimized structures, the performances of the DFT, DFTB1 and DFTB2 methods are not found to be significantly different. They all are found to maintain well the sufficient amount of free space around the rotator, indicating no abnormal inward approaching of the peripheral arms takes place while their computational convergence criteria were on the fly. Additionally, the performances of these methods based on their quantum mechanically derived dihedral angles ϕ responsible to depict the angular orientation of the central rotator in respect to the spin axis and peripheral arm are in the acceptable range. But, relatively, the DFTB2 is found to determine more accurate ($\phi = 0.63\pi$) yet X−ray ($\phi = 0.56\pi$) & DFT ($\phi = 0.63\pi$) reproducible value than that by the DFTB1 ($\phi = 0.68\pi$). As a whole, while comparing the *Jmol* rendered optimized 3D electronic structures of the isolated ROT−2F molecule (Fig. 2) (the DFT derived electronic structure is not shown here as this study focusses mainly the performance evaluations of the DFTB methods) produced by the DFTB1 and DFTB2 quantum mechanically to each other, no significant structural dislocations and steric methyl groups disruptions plus the abnormal alignment of the central rotator along the spin axis are observed. The structural resemblance between Figures 2a and 2b confirms that both of the DFTB methods semiquantitatively derives somewhat same structural geometry under isolated molecular condition. But, meanwhile, some of the structural discrepancies yet quantum mechanically more precise structural datasets that were observed in the DFTB2 produced electronic structure are due to its in−built SCC type computational formulations and unique mathematical treatments to the heteroatomic molecular system such as ROT−2F. By considering the state-of-art mathematical formulations and quantum mechanical approximations of the $DFTB^+$ targeted mainly to address the solid state crystalline molecular systems properly, the performances of the DFTB1 and DFTB2 methods could be practically more comparable yet distinguishable while applying them explicitly to the same crystal structure of ROT−2F, but under PBC (crystalline condition) with and without "dispersion energy corrections" features. The in−depth explanations for the same are given quantitatively in the following subsection 3.1.2.

3.1.2 In reference to Optimized Geometries under Crystalline (PBC) Condition

As per the $DFTB^+$ parser codes and its quantum mechanical approximations, the DFTB1 and DFTB2 methods are especially designed to incorporate the unique computational features compatible to the solid state crystalline molecular systems. However, based on their quantum mechanical formulations, they do perform dissimilarly while applying to the heteroatomic crystalline molecular systems such as ROT−2F molecular compass constituted by the widely varied electronegative atoms C, H, O, Si, and F bonded to each other. Herewith, the in−depth explanations of the performance evaluations of them under PBC are presented in reference to the potential geometrical descriptors including the compass parts of the molecular compass: rotator, stator, spin axis, free−volume, and the rotator's alignment dispensing dihedral angle (ϕ). More particularly, in this subsection, the additional feature "dispersion energy corrections" implemented DFTB2 scheme's computing abilities are compared quantitatively with the DFTB1 and DFTB2 under PBC only scheme. All the measured values of them in the respectively derived *Jmol* rendered unit−cell structures of the ROT−2F are listed in Table 2 where the concerned bond lengths, bond angles, free−volume unit, and dihedral angles ϕ are explicitly tabulated in standard scales. As explained earlier in the subsection 3.1.1, the degree of aromaticity and electronic delocalizations of the central rotator are theoretically confirmed even under the crystalline condition (PBC). All the

methods are found to be able enough to derive the intermediate ranged C–C bond length ($l_{C-C} = 0.14$Å). The more unique yet quantum mechanically standard, and the X–ray derived datasets matching numeral values revealed through the "DFTB2 + PBC + dispersion energy corrections" scheme are due to its van der Waals type intra–molecular (interactions between the rotator and stator) and inter–molecular (interactions between the periodically arranged molecules) forces addressing capabilities via the in–built computational Slater–Kirkwood polarization atomic model. Similarly, the "DFTB2 + PBC + dispersion energy corrections" predicted datasets of each siloxaalkane arm seem almost the duplicated datasets of the X–ray. Unlike by the DFTB1 under PBC, the DFTB2 is able enough to determine even the Si–O bond lengths of all the three siloxaalkane arms more accurately with utmost reproducibility despite its predominant partial π double bond characters which in fact made both the theoretical and experimental schemes to set the Si–O bond on shorter length than the usual. For this convergence efficiency, the exceptional credit goes to the SCC type computing features of the DFTB2 which actually enables us to incorporate the electronic resonance effects and Mulliken atomic charges interactions into its self-consistent iterative procedures practically, and to derive the corresponding nuclear forces with significant accuracy promptly. But, some inconsistencies ($\theta = 0.76\pi$ (DFTB1 + PBC), $\theta = 0.78\pi$ (DFTB2 + PBC), $\theta = 0.77\pi$ (DFTB2 + PBC + dispersion energy corrections)) though are still observed in the X–ray produced Si–O–Si bond angles ($\theta = 0.88\pi$), they all lie in the satisfactory range in regard to the quantum mechanical approximations adopted to model the DFTB$^+$ in order to treat the partial ionic and double bond characters as present in −Si−O−Si− linkages, and to address the related long range non–bonding interactions [39]. Similarly, unlike in non-crystalline molecular condition (subsection 3.1.1), the X–ray derived bond length datasets for the concerned heteroatomic C–Si bond

Table 2. Comparison between DFTB2 and DFTB1 optimized structural parameters of ROT−2F molecular compass under

Molecular Compass (ROT−2F)	Bond lengths (*nm*)	Experimental/Theoretical methods (PBC = Yes)			
		X–ray	DFTB1	DFTB2	DFTB2 + "dispersion energy corrections"
Rotator (difluorophenylene)	C−F	0.144	0.141	0.137	0.137
	C−C	0.138	0.140	0.141	0.140
	C−H	0.093	0.110	0.110	0.110
Stator (Siloxaalkane arm)	C−C	0.153	0.153	0.152	0.152
	C−H	0.097	0.109	0.110	0.110
	C−Si	0.188	0.189	0.186	0.188
	Si−O	0.163	0.175	0.165	0.164
	∠Si−O−Si (avg.)	0.88π	0.76π	0.78π	0.77π
Spin axis	C1−Si1	0.189	0.187	0.187	0.187
	C4−Si2	0.189	0.187	0.187	0.188
"Free−volume" (d_{OF}) (nm)	*d1*	0.510	0.517	0.530	0.478
	d2	0.840	0.767	0.758	0.814
	d3	0.950	0.915	0.911	0.919
Rotator's dihedral angle (φ)	All the atoms involved in it are defined in Fig. 1	0.56π	0.44π	0.395π	0.505π

crystalline condition with and without "dispersion energy corrections".

spin–axis are very accurately reproduced by the both DFTB2 and DFTB1 under PBC with and without "dispersion energy corrections". For this, the substantial recognitions go to their PBC incorporating features and the crystalline molecular assembly associating mathematical formulations plus the perturbation treatments abilities of the tightly bound heteroatomic electronic
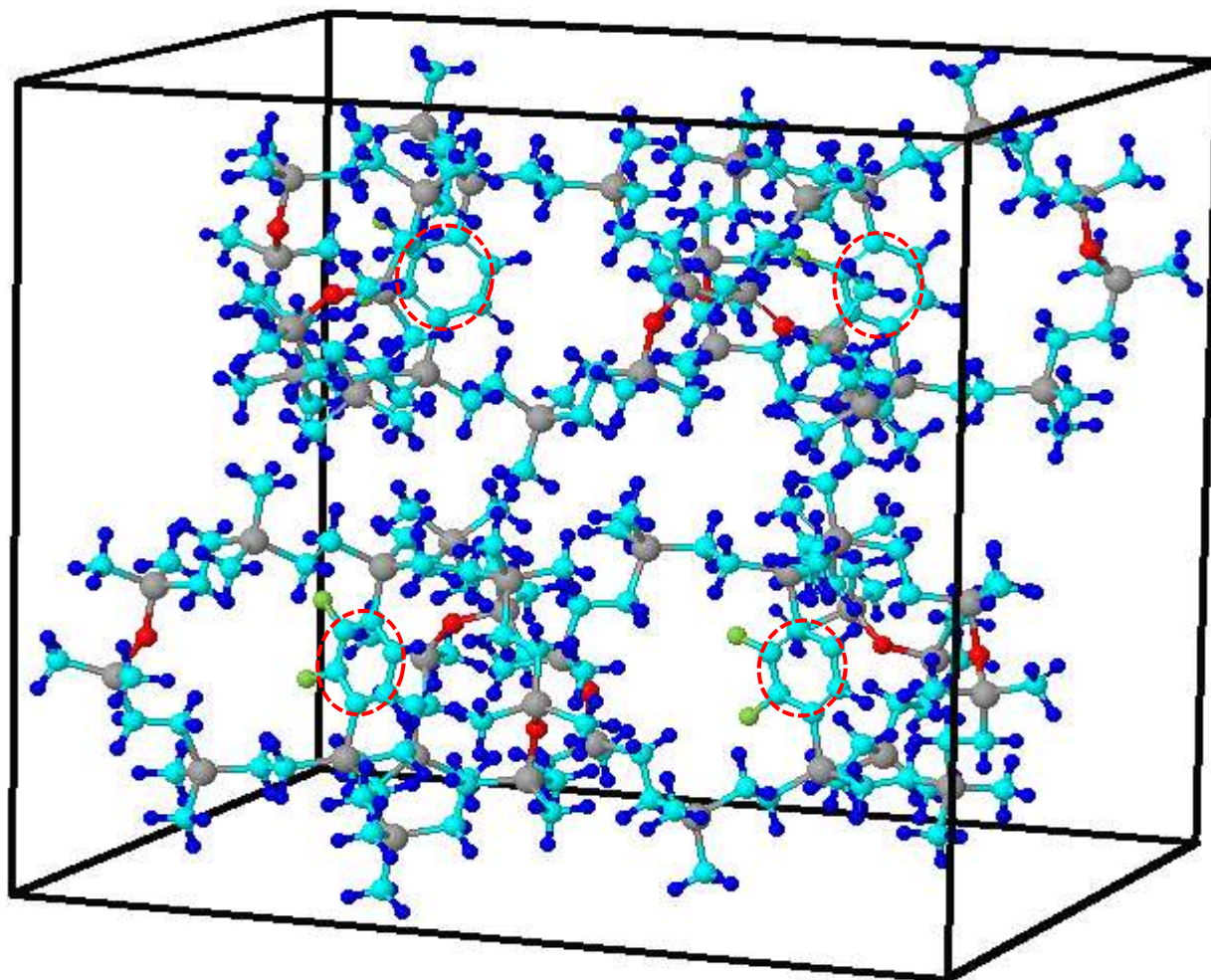

Fig.3. The *Jmol* rendered "DFTB1 + PBC" optimized electronic structure ($\phi = 0.44\pi$ radian) of the ROT–2F unit-cell. The green, blue, dark gray, red, and cyan spheroids represent F, H, Si, O, and C atoms respectively. The boundbox of the unit-cell is also displayed to show the molecular projections along its lattice vectors. The difluorophenylene rotator of each molecular compass is encircled by the red colored shape.

interactions [39]. Moreover, the free–volume unit $d_{OF} = \{d1, d2, d3\}$ datasets computed by the DFTB2 under PBC are found to be quantum mechanically more standard, and they are of course very obvious; but with the inclusion of the "dispersion energy corrections" features, further more standard, accurate, and X–ray produced values reachable datasets are observed as we see in Table 2. Fortunately, none of the distances $\{d1, d2, d3\}$ (measure the space exists in between 'O' atom of each siloxaalkane arm and the nearest 'F' atom of the central rotator) estimated through either of these two methods are found to be deviated abnormally to that of the X–ray derived datasets. It means, the molecular gyroscope/compass needed free space around its rotating segment is well maintained throughout the entire molecular assemblies, marking the extraordinary computing and convergence abilities of the DFTB$^+$ under PBC more especially the DFTB2 even while undertaking "dispersion energy corrections" features programmatically. Additionally, the "DFTB2 + dispersion energy corrections" predicted dihedral angle ($\phi = 0.505\pi$) of the central rotator provides an exceptional evidence to stand it as an extraordinarily performed quantum mechanical scheme as this angular value seems far closer to that of the X–ray observed value ($\phi = 0.56\pi$) than that estimated by the DFTB1 ($\phi = 0.44\pi$) and DFTB2
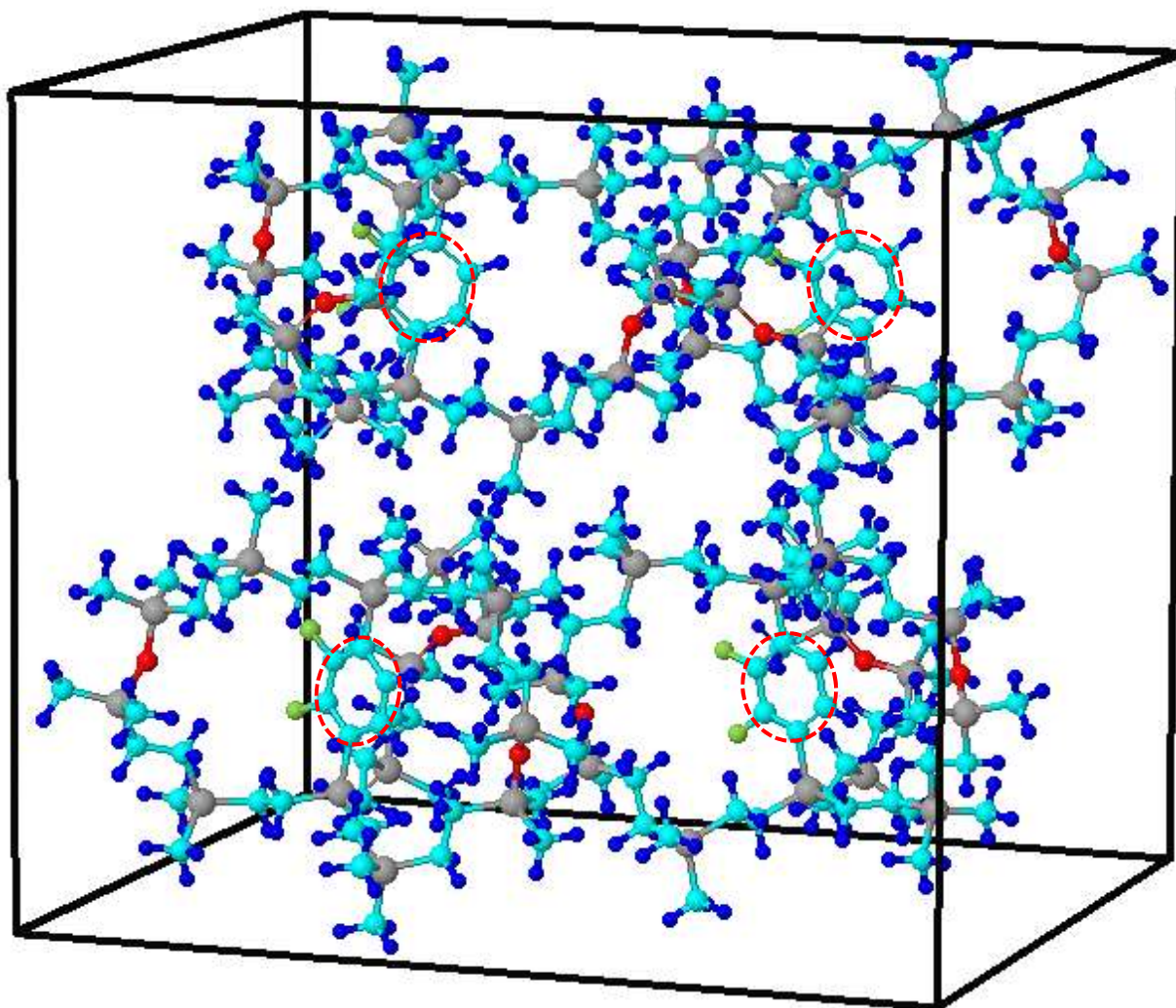
Fig.4. The *Jmol* rendered "DFTB2 + PBC" optimized electronic structure ($\phi = 0.395\pi$ radian) of the ROT$-$2F unit-cell. The green, blue, dark gray, red, and cyan spheroids represent F, H, Si, O, and C atoms respectively. The boundbox of the unit-cell is also displayed to show the molecular projections along its lattice vectors. The difluorophenylene rotator of each molecular compass is encircled by the red colored shape.

($\phi = 0.395\pi$) with PBC features only. These dihedral angles recorded in their own low energy ground state equilibrium structures actually measure one of the flipping positions of the difluorophenylene rotator into the cage center of ROT$-$2F molecular compass practically, and hence stands as a valuable credential to verify its X$-$ray and ^{1}HNMR observed $1\pi-$flipping rotation theoretically. The more descriptive and comprehensive inquiries required to support these observations can only be assessed after consulting with the potential energy surfaces derived through the respective DFTB$^+$ methodologies (subsection 3.1.3). Lastly, for the purpose of carrying out an entire geometrical resemblance between the unit$-$cells derived through the DFTB1 and DFTB2 under PBC, but without and with "dispersion energy corrections", the respectively derived equilibrium electronic structures are displayed in Fig. 3, 4, and 5. As a whole, neither the remarkable variations in the projections of the molecules (number of molecules $Z = 4$) inside the unit$-$cell boundaries nor the abnormal alignment of them along the three dimensional lattice vectors are observed significantly. Meanwhile, the decisive numeral values of the dispersion constants for the H, C, O, Si, and F atoms, and their principal roles in incorporating the effect of intra$-$ and inter$-$ molecular forces of interactions fully for generating such a semiquantitatively reproduced unit$-$cell geometries are discussed in subsection 3.1.3.
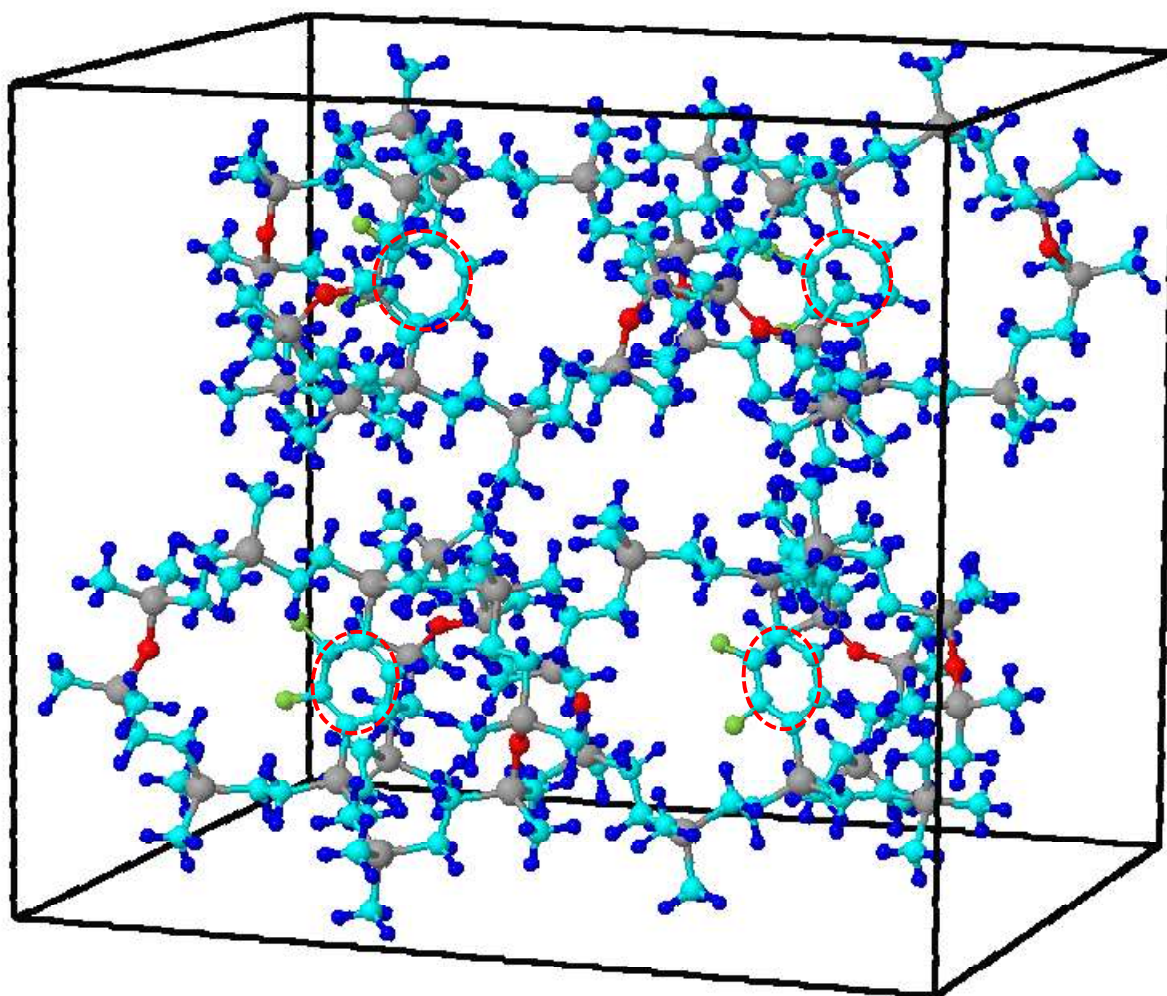
Fig.5. The *Jmol* rendered "DFTB2+ PBC + dispersion energy corrections" optimized electronic structure (ϕ = 0.505π radian) of the ROT−2F unit-cell. The green, blue, dark gray, red, and cyan spheroids represent F, H, Si, O, and C atoms respectively. The boundbox of the unit-cell is also displayed to show the molecular projections along its lattice vectors. The difluorophenylene rotator of each molecular compass is encircled by the red colored shape.

3.1.3 In reference to Molecular Energetics (Potential Energy Surfaces (PESs))

In quantum mechanics, the mathematical relationship between the chemical system's Eigen value E and the specifically selected geometrical coordinates of the atomic nuclei is usually defined by the potential energy surface (PES). It is a unique energy−representation useful mainly to search the pathways for the specific events (in this case, rotary route), the rotary parameters, and other closely associated chemical phenomena plus to determine the activation energy barrier E_a responsible for providing atomic−scale insights into the rotary dynamics [40]. In this study, the *Gaussian−external* methodology operated quantum mechanical methods (DFTB1 and DFTB2) derived Eigen value E at each specific unit−cell geometry of the ROT−2F molecular compass constrained to the predefined dihedral angle ϕ of its dipolar rotator (compass needle) supplied programmatically through the *Gaussian's* PES scanning technique is plotted as a function of ϕ (Fig. 6), and determined the concerned rotational energy barrier E_a, 1π−flipped positions of the rotator, and the symmetric/asymmetric type surfaces quantitatively. Based on the same parameters, the performances of these two DFTB methods are evaluated explicitly while employing them under PBC with and without "dispersion energy corrections". By considering their in-built quantum mechanical formulations plus the extended features applicable mostly to the solid state crystalline molecular systems, the DFTB1 was employed under PBC only whereas the DFTB2 was employed under PBC with and without "dispersion energy corrections"
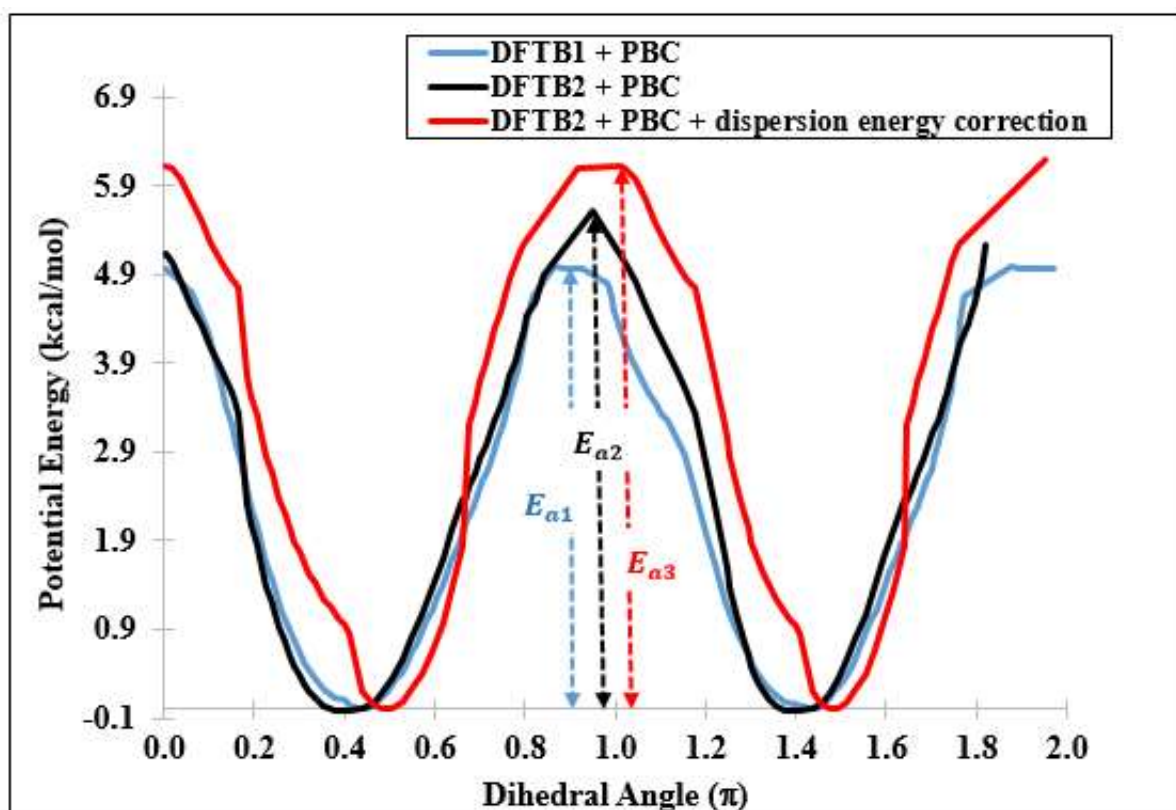
Fig.6. The DFTB1 and DFTB2 derived potential energy surfaces (PESs) of the crystalline molecular compass ROT−2F. The "DFTB2 + PBC + dispersion energy corrections" derived PES is also plotted for the quantitative comparisons. The respective methods estimated rotational energy barriers are denoted by E_{a1}, E_{a2}, and E_{a3}. The dispersion constants for the F atom were supplied as: r_c = 3.8Å, α = 3.4Å^3, and Z^* = 3.5au, and those for the H, O, Si, and C atoms were directly adopted from the ref [14, 25–27], and DFTB$^+$ manual ref [33] (Appendix E; p. 67).

algorithm (Slater–Kirkwood dispersion model). Out of the three potential dispersion constants polarizability α (Å^3), cutoff r_c(Å), Slater–Kirkwood effective numbers N_{eff} dependent nuclear charges Z^*required for addressing van der Waals dispersions correctly, the former two (α (Å^3), and r_c (Å)) for the F atom were set here as variables, and computed the specific potential energy at each dihedral angle ϕ of the rotator constrained in between 0.0π to 0.7π. The respective potential energy vs dihedral angle ϕ plots are shown in Fig. 7(A) and 7(B). While the specific numeral values of each of these constants for the H, O, and C atoms are available in the DFTB$^+$ manual [33] itself, and for the Si atom, they are already tested and reported elsewhere [14] by the same author, the manually unobtainable and even the DFTB$^+$ undeliverable α (Å^3), and r_c (Å) constants for the F atom became the variables to be examined quantitatively. And, meanwhile, due to being the latter constants N_{eff} and Z^* relatively less important in entire SCC iterative computations as they represent long range effective dispersion coefficients and hybridization independent effective atomic charge respectively [33, 34], they were intentionally excluded from the list of the experimental variables; instead set their value for the F atom as; N_{eff} = 3.50; a directly obtainable value from the Halgren relation $N_{eff} = 1.17 + 0.33n_v$ [41], where n_v stands for the number of valence electrons (n_v for F = 7), and therefore is the value of Z^* as 3.50au.

As observed in the ROT−2F's rotational PESs of Fig. 6 derived through the "DFTB1 + PBC" (blue colored line), the activation energy barrier E_{a1}, thematically called rotational energy barrier of the difluorophenylene rotator here, is estimated as E_{a1} = 4.88 kcal/mol. This value is reached to the range of E_{a3} = 5.99 kcal/mol, and E_{a2} = 5.52 kcal/mol while applying DFTB2 under PBC with and without "dispersion energy corrections". The former model underestimated the rotational energy barrier by about ΔE_1 ($E_{a3} - E_{a1}$) = 1.11 kcal/mol, and ΔE_2 (($E_{a2} - E_{a1}$) = 0.64 kcal/mol respectively to that of the DFTB2, and the DFTB2 itself underestimated ΔE_3 ($E_{a3} - E_{a2}$) = 0.47 kcal/mol energy before including "dispersion energy corrections". It means the DFTB2

method determined more reliable and standard energy barriers owing its potential features more compatible to the heteroatomic solid state crystalline molecular systems, and further showed its precision level appreciable and computing skills outstanding after incorporating the dispersive forces (in this case, the interactions between the phenylene rotator and surrounding spokes (intramolecular) plus the interaction between the periodically arranged molecular compasses (intermolecular)) addressing Slater−Kirkwood atomic model. Besides this, the positions of the two low energy states 'global minima', and the single high energy state 'transition state' (#TS) are also not fully reproducible: the "DFTB1 + PBC" scheme determined the first minimum at rotator's dihedral angle $\phi = 0.44\pi$ radian whereas the DFTB2 predicted the same structure at $\phi = 0.505\pi$, and $\phi = 0.395\pi$ radians after implementing PBC with and without "dispersion energy corrections". Their corresponding degenerate 1π−flipped rotator structures are observed at $\phi = 1.44\pi$, $\phi = 1.493\pi$, and $\phi = 1.397\pi$ radians respectively. If they are compared to the positions of experimentally observed 1π−flipped minima at $\phi = 0.56\pi$, and $\phi = 1.56\pi$ radians, the performance of "DFTB2 + PBC + dispersion energy correction" scheme to converge the corresponding structures seems more better and precise than the others even though they all are able to locate the 1π−flipped positions of the rotator with fully converged degenerate electronic structures explicitly. Likewise, the angular positions of the #TS computed by the DFTB1 and DFTB2 are observed at 0.93π, and 0.96π radians under PBC only, but shifted to the higher value at 1.02π radian after including "dispersion energy corrections" features into the latter scheme. In terms of deriving symmetric or asymmetric type PESs, the performances of the DFTB1 and DFTB2 methods are however, agreeable. Both of them accurately reproduced the symmetric type PESs as did by the "DFTB2 + PBC + dispersion energy corrections" scheme. This type PES provides one of the most prominent theoretical evidences for justifying the experimentally observed facile 1π rotation of the central dipolar rotator (compass needle) along the C−Si bond spin axis (Fig. 1(B)) without experiencing any structural blockages from the surrounding siloxaalkane spokes, and any unequal energy obstacles for exhibiting both clockwise (first minimum ($\phi = 0.505\pi$) → second minimum ($\phi = 1.493\pi$)) and anticlockwise (second minimum ($\phi = 1.493\pi$) → first minimum ($\phi = 0.505\pi$)) flipping motions. It ensures us that an exactly equal magnitude of any sorts of the magnetic/electrical/optical stimuli, and other dipole array inducing dielectric responses is required for driving this dipolar rotator (compass needle) externally; a novel yet indispensable prerequisite for functionalizing the dynamic nanomaterials in the molecular machinery world [42].

As noted above, the geometrically converged structural and transition state positions, unit− cell geometries, and the concerned rotational energy barrier E_{a3} computed through the "DFTB2 + PBC + dispersion energy corrections" scheme are significantly varied to those of the DFTB1 and DFTB2 schemes under PBC only. Such quantum mechanical energetic and structural variations are none other than the predominant effects of van der Waals type dispersive forces. It reflects that the van der Waals interactions between the central difluorophenylene rotator and the surrounding siloxaalkane spokes plus the interactions between the periodically arranged molecular compasses do exist significantly in ROT−2F molecular assembly. Therefore, the concerned numeral values of the dispersion constants r_c (Å), α (Å³), and Z^* for the F atom (unavailable in the DFTB$^+$ manual [33]) used for the entire computational tasks presented above are to be determined with quantitative validations. As shown in Fig. 7(A) and 7(B), they were examined based on the molecular energetics or PESs calculations for the "DFTB2 + PBC" derived unit cell structures. The black solid line (Fig. 7(A) represents the PES of the dispersion constants set for the F atom (a) r_c = 2.8Å, α = 3.8 Å³, and Z^* = 3.5au; red dotted line for (b) r_c = 3.8Å, α = 3.8Å³, and Z^* = 3.5au; and the blue solid line for (c) r_c = 4.8Å, α = 3.8Å³, and Z^* = 3.5au. Interestingly, the blue solid− and red dotted− lined PESs are found as perfectly duplicated to each other even while increasing the r_c value to 4.8Å from 3.8Å, but the black solid−lined PES seems slightly fluctuated while decreasing the r_c value to 2.8Å. Therefore, the standard r_c value for the F atom used throughout this study (both for geometry optimizations and PES scanning techniques) is 3.8Å, which is thematically correct as the r_c stands for the cutoff distance when calculating the two−body interactions programmatically, and the minimum nuclear distance between any two nearest atoms in the entire ROT−2F molecular system is recorded as > 2.8Å. Similarly, while increasing the α value for the F atom slightly to 3.8Å³ from the standard DFT derived 3.4Å³ by keeping other constants same, the variation in the PESs seems negligible as displayed by red colored and blue colored lines respectively in Fig. 7(B). Therefore, the standard α value used for the F atom throughout this study is 3.4Å³. It does make sense since
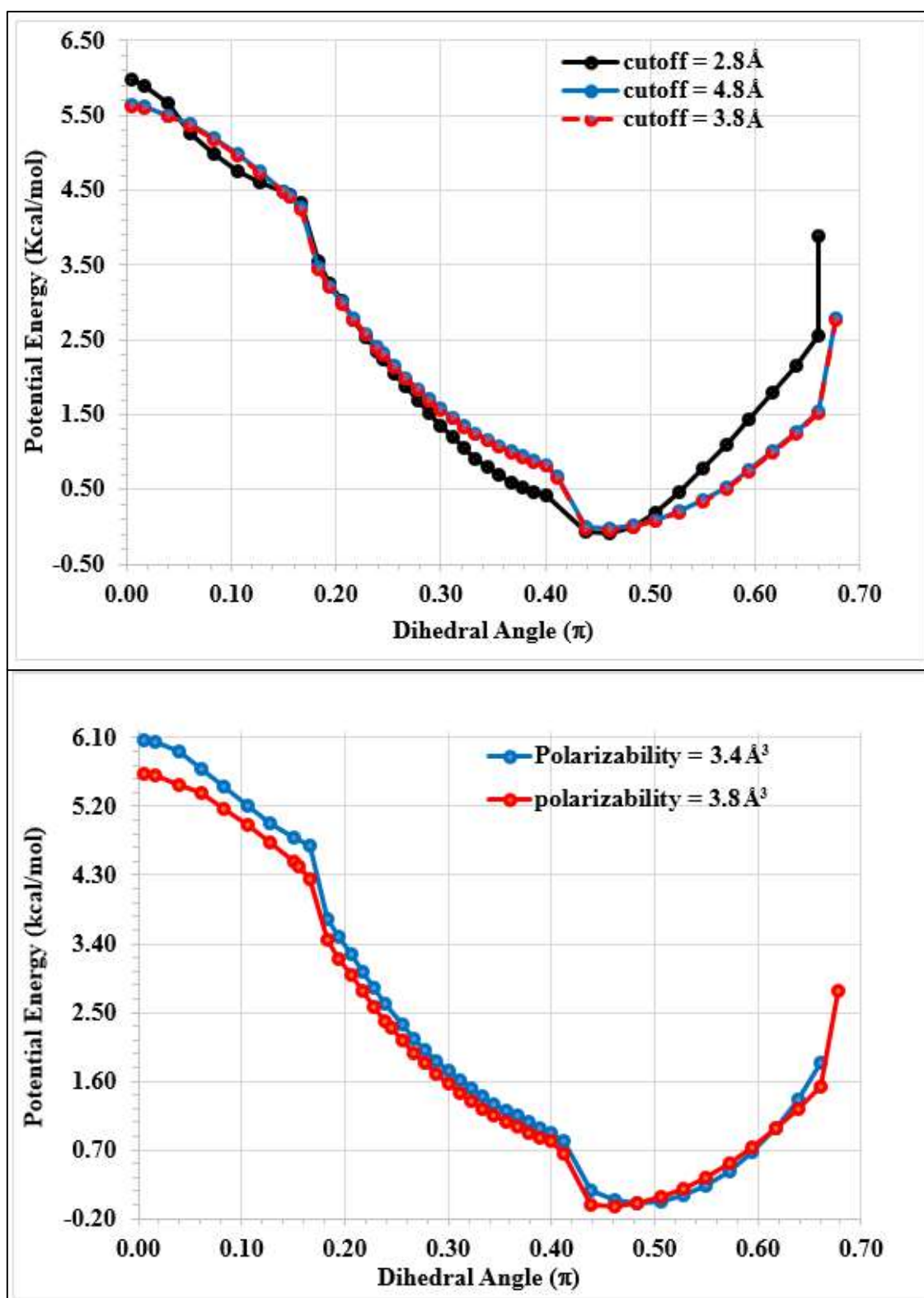
Fig.7. Variations of the "DFTB2 + PBC + dispersion energy corrections" derived potential energy surfaces (PESs) while changing the values of the dispersion constants; (A) cutoff r_c(Å), and (B) atomic polarizability α(Å^3) for the F atom. The set of the constants for H, O, Si, and C atoms are already evaluated elsewhere ref [14, 25–27], and made available in the DFTB$^+$ manual ref [33] (Appendix E; p. 67).

this value is a DFT derived one whose accuracy level is widely taken as equal as *ab initio* methods. All these quantitative illustrations made the present author to state here that the van der Waals energy and the concerned ROT−2F's unit−cell electronic structure are converged well by the "DFTB2 + PBC + dispersion energy correction" scheme whenever the dispersion constants set for the F atom is r_c = 3.8Å, α = 3.4 Å^3, and Z^* = 3.5au. Even with that being said, the point to be noted here is that the DFTB$^+$ adopted van der Waals energy evaluating Slater−Kirkwood dispersion model seems relatively less sensitive to the slight variations in magnitudes of the dispersion constants r_c and α while keeping the Z^* value constant every time. The same was the case while validating the dispersion constants for Si atom earlier by the same author as mentioned elsewhere [14]. It ultimately assures us that the "DFTB2 + PBC + dispersion energy corrections" derived PES (red colored line in Fig. 6) by utilizing r_c = 3.8Å, α = 3.4Å^3, and Z^* = 3.5au numeral values of the dispersion constants for the F atom is accurate enough within the framework of Slater−Kirkwood dispersion model.

IV. CONCLUSIONS

This quantum mechanical study was mainly aimed at evaluating the performances of two quantum mechanically distinct approaches of the density-functional-based tight-binding (DFTB) scheme quantitatively while applying them explicitly to the same heteroatomic amphidynamic crystalline molecular system with macroscopic compass like molecules arranged periodically in the three dimensional crystal lattice. The concerned DFTB models with variable computational parser codes, and dissimilar mathematical formulations and parametrizations were "non-self-consistent-charge" NCC and "self-consistent-charge" SCC based schemes respectively called DFTB1 and DFTB2, and the implemented conditions of them were crystalline (periodic boundary condition (PBC) and non− crystalline (isolated) under the presence and absence of "dispersion energy correction" features, plus the computationally adopted theoretical methodology for functionalizing either of them (external program) under the standardized interface of *Gaussian* by undertaking the external−script fed computational routeway was *Gaussian−external*. The specific crystalline molecular system whose quantum mechanically predicted low energy equilibrium unit−cell geometries and the molecular energetics became the principal bases for their explicit evaluations was the experimentally synthesized siloxaalkane molecular compass ROT−2F with dipolar difluorophenylene segment as a rotator (compass needle), Si−C bonds as a spin axis, and the −Si− & (−Si−O−)$_x$ made siloxaalkane peripheral arms as a stator. Firstly, both the DFTB1 and DFTB2 schemes were applied to the ROT−2F molecular compass under non−crystalline (isolated) condition, and determined its ground state equilibrium geometries followed by their explicit employments under PBC with and without "dispersion energy corrections" for inquiring the concerned unit−cell geometries, experimentally observed 1π−flipped positions of the rotator, rotational energy barriers E_a, nature of the potential energy surfaces (PESs), predominant effects of the van der Waals type dispersion energy and the closely associated dispersion constants, etc. Based on the specifically selected geometrical descriptors (bond lengths, bond angles, dihedral angle, and free−volume unit), and the accessory compass parts (rotator, spin axis, and stator) of the isolated molecular compass plus their quantum mechanically derived absolute magnitudes, the DFTB2 was evaluated as relatively more competitive yet DFT level reachable theoretical scheme than the DFTB1. The more remarkable discrepancies and the distinguishable performances between them were observed while referring to their datasets computed for the same descriptors and compass parts under PBC with and without "dispersion energy corrections". For example, the DFTB2 predicted values for the (a) C−C bond length (l_{C-C} = 0.14Å (intermediate ranged)) of the central difluorophenylene rotator responsible for illuminating its degree of aromaticity and electronic delocalization in a greater extent, (b) C−C, C−H, and C−Si bond lengths of each siloxaalkane arm became the duplicated datasets of the X−ray, and even the Si−O bond length despite its predominant partial π double bond characters; (c) C−Si spin−axis bond lengths became the reproducible values to that of the X−ray; (d) free−volume unit d_{OF} = {$d1$, $d2$, $d3$} representing datasets became the quantum mechanically more standard, accurate, and agreeable to the X−ray produced values, etc. marked itself as an exceptionally outstanding method than the DFTB1. The concerned values for these parameters were produced as more precise after including "dispersion energy corrections" into the DFTB2, and hence, found itself far better than the DFTB2 and DFTB1 run under PBC only. The discrepancies on their performances were more critical and clearly distinctive in their molecular energetic calculations in the form of PESs such as (a) "DFTB1+PBC" estimated the rotational energy barrier of the central rotator as E_{a1} = 4.88 kcal/mol (underestimated by ΔE_1 ($E_{a3} - E_{a1}$) = 1.11 kcal/mol) whereas "DFTB2+PBC" estimated it as E_{a2} = 5.52 kcal/mol (underestimated by ΔE_2 ($E_{a3} - E_{a2}$) = 0.47 kcal/mol) and "DFTB2+PBC+dispersion energy corrections" as E_{a3} = 5.99 kcal/mol.; (b) "DFTB1 + PBC" located the first equilibrium structure (the second 1π−flipped degenerate structure) whenever the rotator's dihedral angle ϕ is equal to 0.44π (ϕ = 1.44π) radian whereas "DFTB2 + PBC" did the same at ϕ = 0.505π (ϕ = 1.493π), and ϕ = 0.395π (ϕ = 1.397π) radians under the presence and absence of

"dispersion energy corrections" features. It means the "DFTB2 + PBC + dispersion energy corrections" determined 1π–flipped degenerate structures of the unit–cell were observed as relatively closer to that of the X–ray derived structures whose similar dihedral angle ϕ were recorded as 0.56π and 1.56π radians respectively. As a whole, the "DFTB2 + PBC + dispersion energy corrections" scheme was evaluated as the most potential and profound quantum mechanical candidate within the framework of DFTB$^+$ parametrizations and its dispersion energy addressing Slater–Kirkwood model, and the "DFTB2 + PBC" scheme stood at the second position performance wise. In the course of evaluating all these computing performances of the DFTB1 and DFTB2 critically, the set of the dispersion constants cutoff r_c (Å), polarizability α (Å^3), and effective nuclear charge Z^*(au) for the F atom (out of H, C, Si, and O atoms) that were actually unavailable in the DFTB$^+$ manual, and most probably undeliberated by any of the DFTB methods so far were also examined quantitatively. The trustworthy numeral values of each of these constants for the F atom determined under the DFTB2 scheme were r_c = 3.8Å, α = 3.4 Å^3, and Z^* = 3.5au respectively. This set of the dispersion constants is expected to be highly useful while applying DFTB2 method to the wide ranged macrocyclic crystalline molecular systems having F as one of the atomic constituents. More importantly, all the justifications and quantitative interpretations conferred throughout this article support the DFBT2 method for nominating itself as the most suitable quantum mechanical scheme in the light of addressing comparatively weaker yet predominantly decisive van der Waals type nonbonding interactions existing mainly in the crystalline molecular solids.

COMPETING INTERESTS

Author has declared that no competing interests exist.

REFERENCES

[1]. Balzani V, Venturi M, Credi A. Molecular Devices and machines: A Journey into the Nano World, Wiley–VCH: Weinheim, Germany, 2003.

[2]. Kelley TR. Molecular Machines. Topics in Current Chemistry, Springer, Berlin, Heidelberg, New York, 2005.

[3]. Dominguez Z, Dang H, Strouse MJ, Garcia–Garibay MA. Molecular "Compasses" and "Gyroscopes." III. Dynamics of a Phenylene Rotor and Clathrated Benzene in a Slipping– Gear Crystal Lattice. Journal of American Chemical Society. 2002; 124(26), 7719–7727. Available: https://pubs.acs.org/doi/10.1021/ja025753v

[4]. Horansky RD, Clarke LI, Price JC, Khuong TV, Jarowski PD, Garcia-Garibay MA. Dielectric response of a dipolar molecular rotor crystal. Physical Review B. 2005; 72: 014302-1–014302-5. Available: https://journals.aps.org/prb/abstract/10.1103/PhysRevB.72.014302

[5]. Horansky RD, Clarke LI, Price JC, Karlen SD, Jarowski PD, Santillan R, Garcia-Garibay, MA. Dipolar rotor-rotor interactions in a difluorobenzene molecular rotor crystal. Physical Review B. 2006; 74:054306-1–054306-12. Available: https://journals.aps.org/prb/abstract/10.1103/PhysRevB.74.054306

[6]. Garcia-Garibay MA, Godinez CE. Engineering Crystal Packing and Internal Dynamics in Molecular Gyroscopes by Refining their Components. Fast Exchange of a Phenylene Rotator by ^{2}HNMR. Crystal Growth & Design. 2009; 9(7):3124–3128. Available:https://mgg.chem.ucla.edu/wp-content/uploads/2021/10/141-CGD-2009-93124 .pdf

[7]. Ellis E, Moorthy S, Chio WK, Lee TC. Artificial molecular and nanostructures for advanced nanomachinery. Chemical Communications. 2018; 54:4075–4090. Available: https://pubs.rsc.org/en/content/articlelanding/2018/cc/c7cc09133h

[8]. Ehnbom A, Gladysz JA. Gyroscopes and the Chemical Literature, 2002–2020: Approaches to a Nascent Family of Molecular Devices. Chemical Reviews. 2021; 121: 3701–3750. Available: https://pubs.acs.org/doi/10.1021/acs.chemrev.0c01001

[9]. Winston EB, Lowell PJ, Vacek J, Chocholousova J, Michl J, Price CJ. Dipolar molecular rotors in the metal–organic framework crystal IRMOF-2. Physical Chemistry Chemical Physics. 2008; 10:5188–5191.

Available: https://www.academia.edu/18877401/Dipolar_molecular_rotors_in_the_met al_organic_framework_crystal_IRMOF_2

[10]. Akimov AV, Kolomeisky AB. Molecular Dynamics Study of Crystalline Molecular Gyroscopes. Journal of Physical Chemistry C. 2011; 115:13584–13591. Available: https://www.academia.edu/14194061/Molecular_Dynamics_Study_of_Crystal line_Molecular_Gyroscopes

[11]. Setaka W, Yamaguchi K. Thermal modulation of birefringence observed in a crystalline molecular gyrotop. Proceedings of the National Academy of Sciences of the USA. 2012; 109:9271–9275. Available: https://www.pnas.org/doi/10.1073/pnas.1114733109

[12]. Setaka W, Ohmizu S, Kabuto C, Kira M. Molecular Gyroscope Having a Halogen-substituted p-Phenylene Rotator and Silaalkane Chain Stators. Chemistry Letter 2010; 39(5), 468–469. Available: https://www.journal.csj.jp/doi/pdf/10.1246/cl.2010.468

[13]. Setaka W, Ohmizu S, Kabuto C, Kira, MA. Molecular Gyroscope Having Phenylene Rotator Encased in Three-spoke Silicon-based Stator. Chemistry Letters 2007; 36(8), 1076 −1077. Available: https://www.journal.csj.jp/doi/epdf/10.1246/cl.2007.1076

[14]. Marahatta AB, Kanno M, Hoki K, Setaka W, Irle S, Kono H. Theoretical Investigation of the Structures and Dynamics of Crystalline Molecular Gyroscopes. Journal of Physical Chemistry C. 2012; 116:24845–24854. Available: https://pubs.acs.org/doi/10.1021/jp308974j

[15]. Marahatta AB. *Gaussian−External* Methodology Predicted Crystal Structures, Molecular Energetics, and Potential Energy Surface of the Crystalline Molecular Compass. Asian Journal of Applied Chemistry Research. 2023; 14(1):8–25. Available: https://journalajacr.com/index.php/AJACR/article/view/255

[16]. Maraatta AB, Kono H. SCC-DFTB Study for the Structural Analysis of Crystalline Molecular Compasses. Chemistry Research Journal. 2022; 7(4):77–94. Available: https://chemrj.org/download/vol-7-iss-4-2022/chemrj-2022-07-04-77-94.pdf

[17]. Marahatta AB, Kono H. Structural Characterization of Isolated Siloxaalkane Molecular Gyroscopes via DFTB-based Quantum Mechanical Model. International Journal of Progressive Sciences and Technologies. 2021; Vol. 26(1):526−541. Available: https://ijpsat.org/index.php/ijpsat/article/view/2950/0

[18]. Marahatta AB, Kono H. Comparative Theoretical Study on the Electronic Structures of the Isolated Molecular Gyroscopes with Polar and Nonpolar Phenylene Rotator. International Journal of Progressive Sciences and Technologies. 2020; 20(1):109−122. Available: https://ijpsat.org/index.php/ijpsat/article/view/1716

[19]. Seifert G. Tight-Binding Density Functional Theory: An Approximate Kohn−Sham DFT Scheme. Journal of Physical Chemistry A. 2007; 111:5609−5613. Available:https://pubs.acs.org/doi/10.1021/jp069056r#:~:text=The%20DFTB%20method% 20is%20an,and%20to%20the%20Harris%20functional.

[20]. Elstner M, Porezag D, Jungnickel G, Elsner J, Haugk M, Frauenheim T, Suhai S, Seifert G. Self-consistent-charge density-functional tight-binding method for simulations of complex materials properties. Physical Review B. 1998; 58:7260−7268. Available: https://journals.aps.org/prb/abstract/10.1103/PhysRevB.58.7260

[21]. Aradi B, Hourahine B, Frauenheim T. DFTB+, a Sparse Matrix-Based Implementation of the DFTB Method. Journal of Physical Chemistry A. 2007; 111:5678−5684. Available:https://pubs.acs.org/doi/10.1021/jp070186p#:~:text=The%20sparsity%20is%20calculated%20as,unique%20am ong%20current%20DFTB%20implementations.

[22]. Elstner M, Frauenheim Th, Kaxiras E, Seifert G, Suhai S. A Self-Consistent Charge Density-Functional Based Tight-Binding Scheme for Large Biomolecules. Physica Status Solidi B. 2000; 217:357−376. Available:https://onlinelibrary.wiley.com/doi/10.1002/(SICI)1521-3951(200001)217: 1% 3C41::AID-PSSB41%3E3.0.CO;2-V

[23]. Elstner M, Porezag D, Jungnickel G, Elsner J, Haugk M, Frauenheim T, Suhai S, Seifert G. Self-consistent-charge density-functional tight-binding method for simulations of complex materials properties. Physical Review B. 1998; 58:7260−7268. Available: https://journals.aps.org/prb/abstract/10.1103/PhysRevB.58.7260

[24]. Marahatta AB, Kono H. Performance of NCC- And SCC- DFTB Methods for Geometries and Energies of Crystalline Molecular Gyroscope. International Journal of Innovative Research and Advanced Studies. 2019; 6(5):180–185. Available: http://www.ijiras.com/2019/Vol_6-Issue_5/paper_28.pdf

[25]. Elstner M, Hobza P, Frauenheim T, Suhai S, Kaxiras E. Hydrogen bonding and stacking interactions of nucleic acid base pairs: a density-functional-theory based treatment. Journal of Chemical Physics. 2001; 114:5149–5155. Available:https://pubs.aip.org/aip/jcp/article-abstract/114/12/5149/183912/Hydrogen-bonding-and-stacking-interactions-of?redirectedFrom=fulltext

[26]. Miller KJ. Additivity methods in molecular polarizability. Journal of American Chemical Society. 1990; 112:8533–8542. Available: https://pubs.acs.org/doi/10.1021/ja00179a044

[27]. Kang YK, Jhon MS. Additivity of atomic static polarizabilities and dispersion coefficients. Theoretica Chimica Acta. 1982; 61:41–48. Available: https://link.springer.com/article/10.1007/BF00573863

[28]. (a) Zheng G, Irle S, Morokuma K. Performance of the DFTB method in comparison to DFT and semiempirical methods for geometries and energies of C_{20}–C_{86} fullerene isomers. Chemical Physics Letter. 2005; 412: 210−216. Available: https://www.sciencedirect.com/science/article/abs/pii/S0009261405009334

(b) Ohta Y, Okamoto Y, Irle S, Morokuma K. Single-walled carbon nanotube growth from a cap fragment on an iron nanoparticle: Density-functional tight-binding molecular dynamics simulations. Physical Review B. 2009; 79:195415 (1−7). Available: https://journals.aps.org/prb/abstract/10.1103/PhysRevB.79.195415

[29]. Koehler C, Seifert G, Gerstmann U, Elstner M, Overhof H, Frauenheim T. Approximate density-functional calculations of spin densities in large molecular systems and complex solids. Physical Chemistry Chemical Physics. 2001; **3**, 5109–5114. Available: https://pubs.rsc.org/en/content/articlelanding/2001/cp/b105782k/unauth

[30]. Lee KH, Schnupf U, Sumpter BG, and Irle S. Performance of Density-Functional Tight-Binding in Comparison to Ab Initio and First-Principles Methods for Isomer Geometries and Energies of Glucose Epimers in Vacuo and Solution. ACS Omega. 2018; 3(12):16899–16915. Available:https://www.ncbi.nlm.nih.gov/pmc/articles/PMC6643604/#:~:text=On%20the%20basis%20of%20a,hydrogen%20bonds%20and%20isomer%20energies.

[31]. Barnett CB, Naidoo KJ. Ring Pukering: A Metric for Evaluating the Accuracy of AM1, PM3, PM3CARB-1, and SCC-DFTB Carbohydrate QM/MM Simulations. Journal of Physical Chemistry B. 2010; 114:17142–17154. Available: https://pubs.acs.org/doi/full/10.1021/jp107620h

[32]. (a) Macrae CF, Edgington PR, McCabe P, Pidcock E, Shields GP, Taylor R, Towler M, van de Streek J. Mercury: visualization and analysis of crystal structures. Journal of Applied Crystallography. 2006; 39:453–457. Available: https://onlinelibrary.wiley.com/doi/abs/10.1107/S002188980600731X

(b) Jmol: An open-source Java viewer for chemical structures in 3D. Available: http://www.jmol.org/

[33]. DFTB⁺ Version 1.3 User Manual. Available: https://dftbplus.org/fileadmin/DFTB-Plus/public/dftb/current/manual.pdf

[34]. Aquilanti V, Cappelletti D, Pirani F. Range and strength of interatomic forces: dispersion and induction contributions to the bonds of dications and of ionic molecules. Chemical Physics. 1996; 209(2–3): 299-311. Available: https://www.sciencedirect.com/science/article/abs/pii/0301010496001632

[35]. Frisch MJ, Trucks GW, Schlegel HB, Scuseria GE, Robb MA, Cheeseman JR, Montgomery JA, Vreven T, Kudin KN, Burant JC.; et al. (2004). Gaussian 03, revision E.01; Gaussian, Inc. Wallingford, CT. Available: https://gaussian.com/g03citation/

[36]. Richard GJ, Julian C. Silicon-Containing Polymers: The Science and Technology of Their Synthesis and Applications", Springer publication, 2000.

[37]. Takao T, Tetsuya T. π-Stacking on Density Functional Theory: A review; 2013. Availale: file:///C:/Users/User/Downloads/review.pdf

[38]. Koskinen P, Mäkinen V. Density-functional tight-binding for beginners. Computational Materials Science 47 (2009) 237–253. Available: https://www.sciencedirect.com/science/article/abs/pii/S0927025609003036

[39]. Kwon HY, Morrow Z, Kelley CT, Jakubikova E. Interpolation Methods for Molecular Potential Energy Surface Construction. Journal of Physical Chemistry A. 2021; 125(45): 9725–9735. Available: https://pubs.acs.org/doi/10.1021/acs.jpca.1c06812

[40]. Halgren, T. The representation of van der Waals (vdW) interactions in molecular mechanics force fields: potential form, combination rules, and vdW parameters. Journal of American Chemical Society. 1992; 114(20):7827−7843. Available: https://pubs.acs.org/doi/10.1021/ja00046a032

[41]. Luo W, Wang N, Li HK, Xu ZJ, Feng Y, Fu X, Shi C, Ye HY, Miao LP. Fast rotating dipole array inducing large dielectric response in a Ruddlesden–Popper hybrid perovskite ferroelastic. **Inorganic Chemistry Frontier**. 2023; **10**:5082−5088.